

PREDICTION OF RUN-OUT PROCESS FOR A DEBRIS FLOW TRIGGERED BY A DEEP RAPID LANDSLIDE

Y. NISHIGUCHI(*), T. UCHIDA(*), K. TAMURA(*) & Y. SATOFUKA(**)

(*) Public Works Research Institute, Ibaraki, Japan

(**) Department of Civil Engineering, Ritsumeikan University, Shiga, Japan

ABSTRACT

Previous studies have shown that numerical simulation models commonly used for debris flows may not be applicable for large-scale debris flows. In this study, we developed a technique for simulation of large-scale stony debris flows. For this purpose, we tested the hypothesis that the motion of fine sediment in these debris flows is similar to that of the interstitial water. We developed key parameters to simulate large-scale debris flows, such as sediment concentration, fluid density, and representative particle diameter based on the hypothesis. We also used a modified version of the continuity equation for sediment in our simulation. We conducted detailed field surveys of a past debris flow in Japan and used topographic data from LiDAR imagery, porosity measurements of soil and weathered bedrock, and the grain size distribution of the debris flow sediments to test our model. We also proposed a new process-based method for determination of hydrographs at the lower end of the landslide scar. Using these new data and methods, we conducted numerical simulations of the past debris flow, which reproduced well the observed erosional and depositional pattern if when the concept of fine sediment behaving like fluids was included in the numerical simulation.

KEY WORDS: debris flow, deep rapid landslide, numerical simulation

INTRODUCTION

Landslides induced by rainstorms or earthquakes often have disastrous implications for human society. In particular, deep rapid landslides have triggered large-scale debris flows that have had serious impacts on humans. Therefore, it is important to predict the run-out process of debris flows and to identify debris flow hazard areas. A number of numerical simulation models have been developed to describe the propagation and deposition of debris flows (e.g., EGASHIRA *et alii*, 1989; O'BRIEN *et alii*, 1993; TAKAHASHI & KUANG, 1986; IVERSON & DENLINGER, 2001; TAKAHAMA *et alii*, 2002; RICKENMANN *et alii*, 2006). However, useful techniques for the prediction of run-out processes for large debris flows have not yet been developed.

Most models used to describe stony debris flows assume that they consist of solid and fluid phases (TAKAHASHI, 1977). In models of this type, if the river bed or hill slope is stable, both sediments and interstitial water are assumed to be stationary (Fig. 1a). When sediments move in a debris flow, their motion under these models is considered to be laminar, while that of the interstitial water is turbulent (HOTTA *et alii*, 1998) (Fig. 1b), so these models comprise a "solid phase" of sediments exhibiting laminar flow and a "fluid phase" of interstitial water exhibiting turbulent flow.

Most of these models assume that all sediments are the same size. However, real large-scale debris flows have a broad grain size distribution; numerical simulations based on these simplified models may be

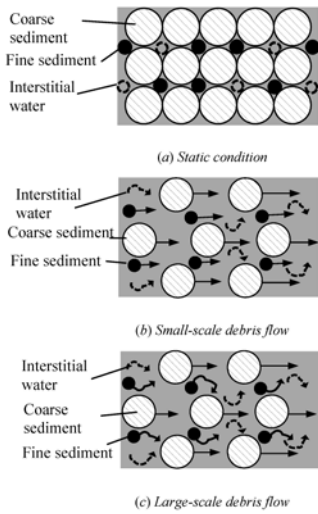


Fig. 1 - Conceptual diagram of static condition, small-scale debris flow and large-scale debris flow

inappropriate for large-scale debris flows. ASHIDA & EGASHIRA (1985) argued that the motion of fine sediments in a large-scale debris flow triggered by a large landslide at Mt. Ontake in Nagano in 1984 could be represented by a fluid phase, whereas the motion of the coarse sediment was that of a solid phase. Thus, for this large-scale debris flow, both the fine sediments and the interstitial water exhibited turbulent flow, and only the coarse sediment exhibited laminar flow (Fig. 1c). Further, NAKAGAWA *et alii*, (1998) and EGASHIRA *et alii*, (1998) performed numerical simulations of past large-scale debris flows with particular attention to the motion of fine sediments. The results of their simulations matched the observed deposited area and thickness of the debris-flow deposits if it was assumed that increases of fluid density were dependent on the proportion of fine sediments considered as a fluid phase, or when coarse and fine sediments were considered independently to account for their different behaviour and the different continuity equations between coarse and fine sediments were presented.

Although these numerical simulations have provided powerful tools to describe the propagation and deposition of debris flows, most parameters have been determined by back-calculation or by calibration to match field observations; in many cases, mean values have been used. Consequently, the hypothesis that the motion of fine sediments in debris flows is similar to that of interstitial water has not been fully examined.

The objective of our study was to examine the

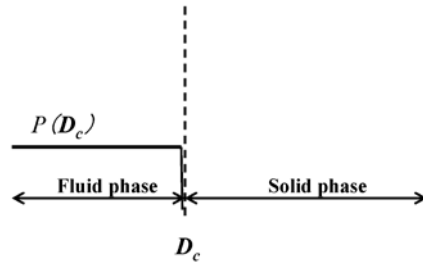


Fig. 2 - Definition of D_c

hypothesis that the motion of fine sediments in debris flows is similar to that of interstitial water, and to develop a valid technique for the simulation of large-scale stony debris flows. To test our hypothesis, we conducted detailed field surveys of debris flows by using topographic measurements from LiDAR data, measuring the porosity of soil and weathered bedrock and measuring the grain size distributions of debris flow sediments. Further, we proposed a new process-based method for the determination of debris flow hydrographs at the lower end of the landslide scar. We also considered the effects of the uncertainty of several parameters on the simulated result.

THEORY

We assumed that the sediments in large-scale debris flows comprise two types of sediments, a coarse sediment and a fine sediment, and that the motion of the fine sediment in a debris flow is similar to that of the interstitial water. We therefore considered these fine sediments as a fluid phase. Further, we defined a maximum diameter D_c for sediments that behave like a fluid (Fig. 2; discussed later). On the basis of this definition of D_c we characterized the key parameters for our numerical simulation; these are sediment concentration at the lower end of the landslide scar (C_d , Eq. 1), fluid density of the debris flow averaged in time and space ($\bar{\rho}$, Eq. 2), and the representative particle diameter of the debris flow (D , Eq. 3).

$$C_d = (1 - w)(1 - P(D_c)) \tag{1}$$

$$\bar{\rho} = \frac{\bar{w}\bar{\rho}_w + (1 - \bar{w})\bar{\rho}_s P(D_c)}{w + (1 - w)P(D_c)} \tag{2}$$



Fig. 3 Location of our study site

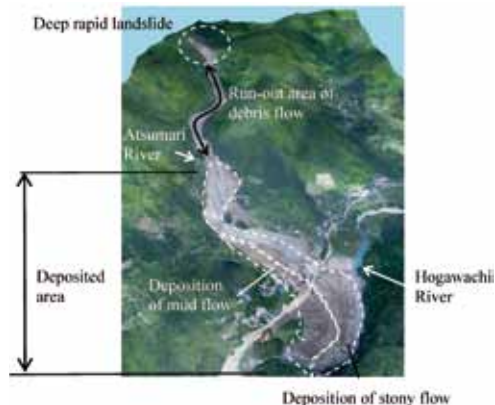


Fig. 4 - Aerial photograph after the debris flow

$$D = d(D_c) \tag{3}$$

where $P(D_c)$ is the ratio of sediment smaller than D_c to all sediment (Fig. 2), ρ_w is water density, ρ_s is the solid density of sediment, $d(D_c)$ is the weighted average particle diameter greater than D_c , w is the water content of landslide soil and bedrock, \bar{w} and \bar{w} is water content of the debris flow averaged in time and space.

We also modified the continuity equation

$$\frac{\partial C_d h}{\partial t} + \frac{\partial C_d u h}{\partial x} + \frac{\partial C_d v h}{\partial y} = i C_s \tag{4}$$

based on our definition of D_c so that

$$\frac{\partial C_d h}{\partial t} + \frac{\partial C_d u h}{\partial x} + \frac{\partial C_d v h}{\partial y} = i C_s (1 - P(D_c)) \tag{5}$$

where t is time, i is erosion and deposition rates, u and v are velocities in the x and y direction, respectively, h is flow depth of debris flow, and C_s is volumetric sediment concentration in the river bed.

MATERIALS AND METHODS

STUDY SITE

The site of this study is Atsumari River in Kumamoto Prefecture, Japan (Fig. 3). Heavy rain on 20 July 2003 induced a deep rapid landslide and the resultant mass of collapsed sediments caused a large-scale debris flow that hit the village along Atsumari River, killing at least 15 people. The study area is underlain by andesite and weathered tuff breccia. The slip surface of the landslide was the interface between

weathered andesite and weathered tuff breccia.

A field survey immediately after the debris flow identified two distinct types of debris flow deposits, muddy deposits and stony deposits (Fig. 4). Local people who were interviewed said that the muddy debris flow occurred first and was followed by the stony debris flow 10–20 min later. The distance from the lower end of the landslide scar to the lower end of the debris flow deposits was about 1,600 m.

According to aerial photographs, LiDAR data and field survey data, the total volume of collapsed sediment was around 42,700 m³, including void volume (hereafter, sediment volume includes void volume), and the volume of collapsed sediment that remained in the landslide scar was 12,220 m³. Therefore, the volume of sediment in the debris flow was about 30,500 m³. Moreover, the volume of sediment eroded from the river bed within the run-out area was estimated to be 59,100 m³. Therefore, the total volume of sediment which reached deposited area was about 89,600 m³. The total volume of the debris flow deposits was estimated to be 76,500 m³, which suggests that 13,100 m³ of sediment flowed further down the Hogawachi River. Although the relative volumes of muddy debris flow and stony debris flow were not measured, aerial photographs and field observations indicate that more than half of the sediment volume was stony debris flow.

FIELD INVESTIGATION

TOPOGRAPHY

Before the debris flow, the run-out area was covered with vegetation, so the width of debris flow in the run-out area was estimated by calculating the differ-

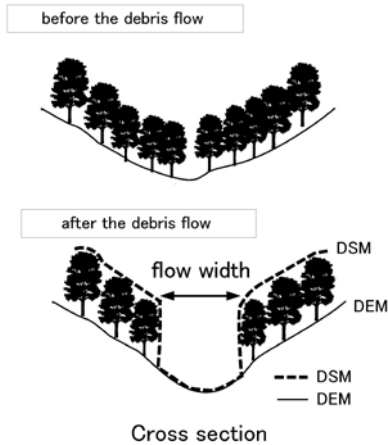


Fig. 5 - Method for calculation of flow width from DEM and DSM

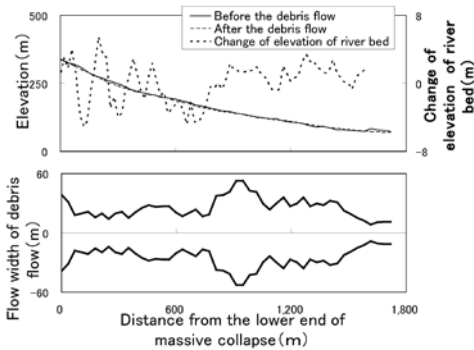


Fig. 6 - Longitudinal profile and width of debris flow

ence between a digital surface model (DSM) and a digital elevation model (DEM), both generated from LiDAR data (Fig. 5). In the depositional area, it was evaluated from aerial photography.

The elevations of the land surface along a longitudinal profile through the debris flow before and after the debris flow were obtained from aerial photography and LiDAR data, respectively. The magnitude of the elevation change was calculated as the difference of these (Fig. 6).

POROSITY OF SOIL AND BEDROCK

Porosity of soil and weathered bedrock of the hill slope were determined from two boreholes near the landslide scar. We measured bulk density and soil water content using a gamma-radiation density gauge and a nuclear radiation moisture gauge, respectively (Fig. 7). Mean porosity of soil and bed-

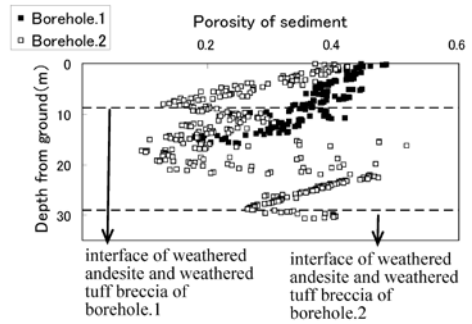


Fig. 7 - Depth profiles of porosity from two boreholes near the landslide scar

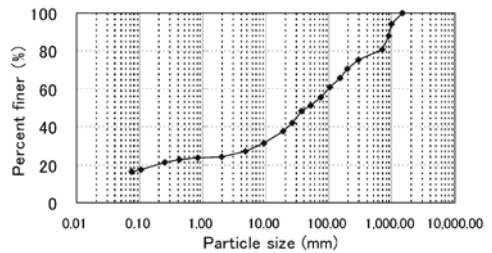


Fig. 8 - Particle size distribution of debris flow

rock from ground surface to landslide slip surface (i.e., the interface between weathered andesite and weathered tuff breccia) was around 0.34.

PARTICLE SIZE DISTRIBUTION OF THE DEBRIS FLOW

We evaluated the particle size distribution of sediments between 7.5 cm and 30 cm from the cross-sectional photograph of the deposits. We also identified the proportions of sediments smaller than 7.5 cm and larger than 30 cm by using the photograph. We combined the sieve test result of sediments smaller than 7.5 cm and the observed result of particle size distribution of sediments larger than 30 cm with the particle size distribution of sediment between 7.5 cm and 30 cm at the rate of their respective proportions (Fig. 8).

NUMERICAL SIMULATION MODEL

We used the “Kanako2D” debris flow simulator, which can simulate 1D debris flows in gullies and 2D debris flows in alluvial fans (NAKATANI *et alii*, 2008). This simulator can be applied to transport of sediments ranging from bed load to stony debris flow. The equations from Eq.6 to Eq.11 are governing equations in the Kanako2D simulation. Eq.6 is continuation

equation for the total volume of debris flow.

$$\frac{\partial h}{\partial t} + \frac{\partial uh}{\partial x} + \frac{\partial vh}{\partial y} = i \tag{6}$$

where i is erosion/deposition rate. Then, the continuation equation for determining the debris flow is as follow.

$$\frac{\partial C_d h}{\partial t} + \frac{\partial C_d uh}{\partial x} + \frac{\partial C_d vh}{\partial y} = i C_s (1 - P(D_s)) \tag{7}$$

Eq.8 is the set of momentum equations for the phenomenon of x-axis direction flow and y-axis direction flow.

$$\begin{cases} \frac{\partial u}{\partial t} + u \frac{\partial u}{\partial x} + v \frac{\partial u}{\partial y} = g \sin \theta_{wx} - \frac{\tau_x}{\rho h} \\ \frac{\partial v}{\partial t} + u \frac{\partial v}{\partial x} + v \frac{\partial v}{\partial y} = g \sin \theta_{wy} - \frac{\tau_y}{\rho h} \end{cases} \tag{8}$$

where g is gravitational acceleration, θ_{wx} and θ_{wy} are flow surface gradients in the x- and y-axis directions, τ_x and τ_y are river bed shearing stresses in the x- and y-axis directions. Then τ_x is described as Eq. 9 (NAKAGAWA *et alii*, 2001).

$$\begin{cases} \frac{\tau_x}{\rho h} = \frac{u\sqrt{u^2 + v^2} d^2}{8h^3 \left\{ C_d + (1 - C_d) \frac{\bar{\rho}}{\rho_s} \right\} \left[\left(\frac{C_s}{C_d} \right)^{1/3} - 1 \right]^2} & \text{if } C_d \geq 0.4 C^* \\ \frac{\tau_x}{\rho h} = \frac{1}{0.49} \frac{u\sqrt{u^2 + v^2} d^2}{h^3} & \text{if } 0.01 < C_d \leq 0.4 C^* \\ \frac{\tau_x}{\rho h} = \frac{g n_m^2 u \sqrt{u^2 + v^2}}{h^{4/3}} & \text{if } C_d \leq 0.01 \text{ or } h/d < \geq 30 \end{cases} \tag{9}$$

where n_m is Manning's coefficient. The river bed shearing stress in y-axis direction is determined when u is replaced by v in Eq.9. Equation for determining change in bed surface elevation is as follow

$$\frac{\partial z}{\partial t} + i = 0 \tag{10}$$

Then, i is described as Eq.11. (NAKAGAWA *et alii*, 2001).

$$\begin{cases} \text{Erosion rate} \\ i = \delta_e \frac{C_s - C_d}{C_s - C_\infty} \frac{q}{d(D_s)} & \text{if } C_s \geq C_d \\ \text{Deposition rate} \\ i = \delta_d \frac{C_s - C_d}{C_s} \frac{q}{h} & \text{if } C_s < C_d, \end{cases} \tag{11}$$

where C_∞ is equilibrium sediment concentration in the debris flow, δ_e and δ_d are coefficients of erosion and deposition rates and q is discharge of debris flow per unit width.

DATA PREPARATION

The simulation covered the area from the lower end of the landslide scar to the lower end of the debris flow deposits. How we determined the main simulation parameters is provided in Table 1.

The longitudinal profile of the river bed and the width of the debris flow were determined from field survey data (Fig. 6). Our field survey data also showed that the maximum erosion depth was 5 m, indicating that the initial depth of the movable bed layer (D_s) was at least 5 m. Bedrock was exposed over much of the eroded area, but movable sediment remained in some areas after the debris flow, suggesting that the mean initial depth of the movable bed layer might have been more than 5 m. Consequently, we used two values (5

Parameter	Method and input data
Longitudinal profile of stream bed elevation	Aerial photography and LiDAR imagery [Fig. 6]
Flow width	Aerial photography and LiDAR imagery [Fig. 6]
Initial depth of movable bed layer (D_s)	Field survey and trial and error [5 and 10 m]*
Water content of soil and weathered bedrock (w)	Borehole data [0.34]
Water content of debris flow averaged in time and space (\bar{w})	Average of observed water content of soil and bedrock source of landslide material and that of river bed material according to previous studies [0.37]
Sediment concentration of debris flow at lower end of landslide scar (C_d)	Formulated equation [Eq. 1]
Fluid density of debris flow averaged in time and space ($\bar{\rho}$)	Formulated equation [Eq. 2]
Fluid density of debris flow at lower end of landslide scar (ρ)	Formulated equation [Eq. 14]
Maximum diameter of sediment that behaves as fluid phase (D_c)	Trial and error [0, 10, 20, 30, and 100 mm]
Representative particle diameter of debris flow (D)	Formulated equation [Eq. 3]
Ratio by volume of stony debris flow to total flow (k)	Trial and error [0.7, 0.5, and 0.9]*

* Values used for trial-and-error determination of the most appropriate value of D_c .

Tab. 1 - Determination of main simulation parameters

and 10 m) for initial depth of the movable bed layer.

Sediment concentration at the lower end of the landslide scar, fluid density and the representative particle diameter of the debris flow were determined from Eqs. 1, 2, and 3, respectively. We assumed that the soil and weathered bedrock of the landslide material were water saturated. Our field investigations at boreholes 1 and 2 showed that porosity of landslide soil and bedrock was 0.34, so we used 0.34 for the water content of soil and weathered bedrock. We determined C_d at the upper end of the simulation area (i.e., at the lower end of the landslide scar) from Eq. 1 with $w = 0.34$.

For our first-order approximation, we assumed that D_c and ρ were constant in both space and time. Therefore, the input value of ρ in the numerical simulation represents the fluid density of the debris flow in the run-out area. According to our field observations, the upper part of the river was eroded by the debris flow, so we assumed that the debris flow was composed of both collapsed sediments and river bed sediments. Therefore, we decided to use an average of the water content of the soil and weathered bedrock that yielded the landslide and that of the river bed materials for w in Eq. 2. Although we did not measure the water content of river bed material, previous studies reported it to be around 0.4, so we used the average of 0.34 and 0.4 (i.e., 0.37) for w in Eq. 2.

We used the observed particle size distribution (Fig. 8) to calculate sediment concentration, fluid density, and the representative diameter of debris flow particles. To ascertain the effect of different values for the maximum diameter of sediment that behaves like a fluid (D_c), we considered five cases ($D_c = 0, 10, 20, 30, \text{ and } 100 \text{ mm}$). Grain size distribution of the debris flow at Atsumari river showed that a large proportion of fine material were included. Although these fine materials might have colloidal properties, in this paper, we did not consider these effects.

To construct a hydrograph at the lower end of the landslide scar, we needed to determine the ratio by volume of stony flow to total flow (k). We used aerial photography and field data to determine that k was between 0.5 and 1.0. Therefore, we used values of 0.5, 0.7, and 0.9 for k in our simulations.

The hydrograph at the lower end of landslide scar (i.e., the upper end of the simulation area) was estimated as follows. Movement of a landslide mass can be expressed as

$$L = v_m t_s, \tag{12}$$

where L is longitudinal length of the landslide scar (120 m), v_m is mean velocity at the lower end of the landslide scar, and t_s is the duration of the landslide at the lower end of the landslide scar.

Mean flow depth at the lower end of the landslide scar (h_m) can be described as

$$h_m = \frac{V_s}{B_m L}, \tag{13}$$

where V_s is total volume of stony debris flow at the lower end of the landslide scar, and B_m is flow width at the lower end of the landslide scar.

Additionally, we assumed that the relationship between velocity and depth of debris flow at the lower end of the landslide scar could be described by the resistance law developed by TAKAHASHI (2004):

$$\frac{v_m}{\sqrt{g h_m I_m}} = \frac{2}{5} \left[\frac{1}{a_i \sin \alpha} \left\{ C_d + (1 - C_d) \frac{\rho}{\rho_s} \right\} \right]^{1/2} \left\{ \left(\frac{C_{d^*}}{C_d} \right)^{1/3} - 1 \right\} \frac{h_m}{d(D_c)}, \tag{14}$$

where I_m is slope angle at the lower end of the landslide scar, a_i and α are constants (0.042 and 17.8° , respectively) (TAKAHASHI, 2004), and C_{d^*} is the maximum possible sediment concentration (0.65). Here, ρ is fluid density at the lower end of landslide scar, which can be described as

$$\rho = \frac{w \rho_w + (1 - w) \rho_s P(D_c)}{w + (1 - w) P(D_c)}. \tag{15}$$

So, the duration of the hydrograph was

$$t_s = \frac{5(a_i \sin \alpha L^5 B_m^3)^{1/2} d(D_c)}{2 \left\{ C_d + (1 - C_d) \frac{\rho}{\rho_s} \right\}^{1/2} \left\{ \left(\frac{C_{d^*}}{C_d} \right)^{1/3} - 1 \right\} (V_s^3 g I_m)^{1/2}} \tag{16}$$

Fig. 9 shows hydrographs for D_c equal to 0, 10, 20, 30, and 100 mm. At the precipitation station near Atsumari River, maximum 10-minute rainfall of 26 mm has been recorded before the debris flows. The water discharge attributed to the rainfall was estimated at 30 m³/s at the upper end of the simulation area, assuming a ratio of rainfall to runoff of 1.0. Discharge of this volume is negligible in comparison to the discharges presented by the hydrographs of Fig. 9. Consequently, we didn't include water discharge attributed to rainfall in the upper drainage area with the hydrographs of Fig. 9.

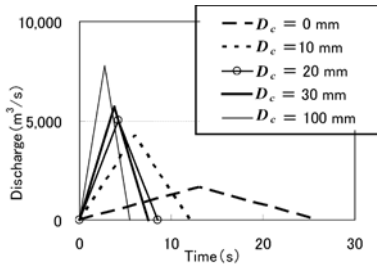


Fig. 9 - Hydrographs for different values of D_c

Values of δ_e and δ_d in Eq. 11 were set as 0.0007 and 0.05 respectively, based on previous studies (NAKATANI *et alii*, 2008; NAKATANI, 2010).

RESULTS

When all sediment particles in the debris flow were considered to behave as solids ($D_c = 0$), the simulated travel distance from the lower end of the landslide scar to the lower end of the debris flow deposits was about 600 m, which is about 40% of the observed travel distance. For this case, there was no erosion by the debris flow and deposition started immediately downstream of the landslide scar. As D_c increased, simulated travel distance of the debris flow increased (Fig. 10). When D_c was larger than 10 mm, the upper part of the stream was eroded. The distance from the lower end of the landslide scar to the lower end of the eroded area (hereafter referred to as “erosion distance”) also increased with increasing D_c . For D_c of 20 mm, the simulated travel and erosion distances and depths of erosion and deposition agreed well with our observations (Fig. 10).

Figure 11 shows the results of simulations for which the ratio of the volume of stony debris flow to total volume (k) and initial depth of the movable bed layer (D_s) were changed, while D_c was fixed at 20 mm. When k is 0.7, the calculated volume and thickness of the deposit well agreed with the observed volume and thickness of the deposit. However, for k in the range from 0.5 to 0.9, the differences of the simulated travel and erosion distances were unremarkable (Fig. 11) which indicates that total volume of sediment at the upper end of the simulation did not influence the erosion and deposition distances of the debris flow, although the erosion and deposition distance were influenced by D_c . Thus, even though there was uncertainty regarding the total volume of sediment at the upper end of the simulation, this uncertainty had little impact on the results of erosion and deposition distances

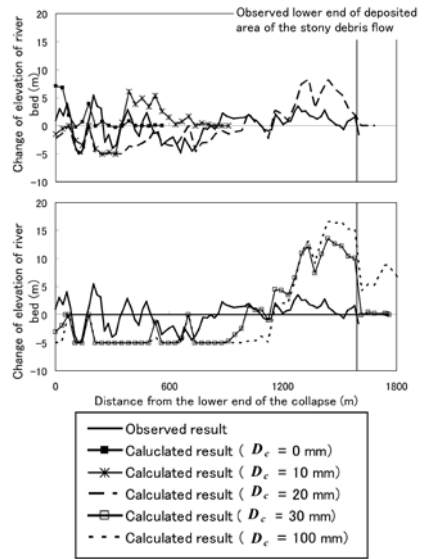


Fig. 10 - Observed and calculated results for different values of D_c

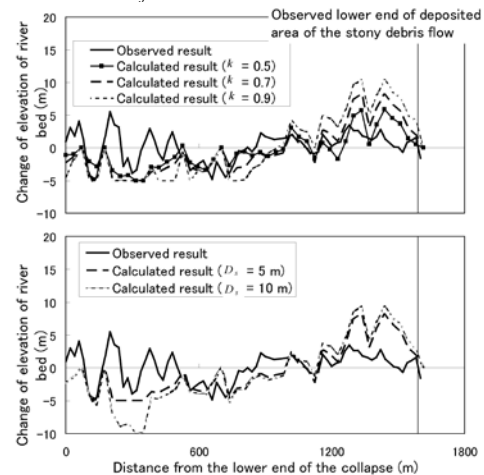


Fig. 11 - Observed and simulated results for different values of k and D_s

of the simulation.

Then, the calculated erosion depth was much larger for D_s of 10 m than for D_s of 5 m and calculated erosion depth well agreed with the observed depth when D_s was 5 m. However, travel and erosion distances were not affected by D_s , although they were influenced by D_c . This indicates the simulated travel and erosion distances for D_c of 20 mm agreed well with the observed result regardless of the value of D_s in the range of 5-10 m. Therefore, the calibrations of k and D_s contributed little to the simulation matching the observed travel and erosion distances.

DISCUSSION

To verify the D_c value of 20 mm, we compared the friction velocity of the debris flow, turbulent velocity of interstitial water, and the settling velocity of sediment of 20 mm diameter.

According to RUBEY (1933), settling velocity (ω_0) can be expressed as

$$\begin{cases} \omega_0 = \sqrt{(\rho_s/\rho - 1)gd(D_c)} F(d) \\ F(d) = \sqrt{\frac{2}{3 + \frac{36\nu^2}{sgd(D_c)^3}} - \frac{\sqrt{36\nu^2}}{\sqrt{sgd(D_c)^3}}} \quad (s = \rho_s/\rho - 1), \end{cases} \quad (17)$$

where ν is kinematic viscosity (0.01 cm²/s). When D_c is 20 mm, ω_0 is 37 cm/s (Table 2).

The friction velocity (U^*) can be calculated from river bed shear stress as

$$U^* = \sqrt{gh_f I_f} \quad (18)$$

Here, we treated h_f and I_f as simulated mean flow depth and mean slope angle, respectively, in the run-out area. As a consequence, U^* was 164 cm/s (Tab. 2).

The turbulent velocity (v_f) can be calculated from turbulent stress (HOTTA *et alii*, 1998).

$$v_f = \sqrt{\frac{\rho_f}{\rho}} \quad (19)$$

where ρ_f is turbulent shear stress, and ρ_f can be expressed as

$$\rho_f = \alpha^2 \rho \frac{25u_f^2}{4h_f^2} d(D_c)^2 \left(1 - \frac{z}{h_f}\right) \quad (20)$$

where u_f and h_f are simulated mean flow velocity and simulated mean flow depth of debris flow, respectively, when D_c is 20 mm. z is bed elevation (here, regarded as 0) and α can be expressed as

$$\alpha = \sqrt{k_f \left(\frac{1 - C_{df}}{C_{df}}\right)^{1/3}} \quad (21)$$

where k_f is an empirical coefficient of 0.16 and C_{df} is the simulated mean sediment concentration of the debris flow when D_c is 20 mm. Then, v_f was determined to be 80 cm/s (Tab. 2).

Consequently, the friction and turbulent velocities were larger than the settling velocity for particles 20 mm in diameter, which verifies that a particle size of 20 mm can be suspended and in turbulent motion in a debris flow. This means that $D_c = 20$ mm was a physi-

cally reasonable assumption.

CONCLUDING REMARKS

Our aim was to develop a technique to simulate large-scale stony debris flows and to examine the hypothesis that the fine sediments in such debris flows behave as fluids. Focusing on the maximum diameter of sediment particles that behave as fluids (D_c), we characterized the key parameters for numerical simulation of the debris flow; these are sediment concentration, fluid density, and representative particle diameter. We also used a modified version of the general continuity equation for sediments. We conducted detailed field surveys and used topographic data from LiDAR imagery, porosity measurements of soil and weathered bedrock, and the grain size distribution of the debris flow sediments to test our model. Further, we proposed a new process-based method for determination of hydrographs of a debris flow at the lower end of the landslide scar. We also considered the effect of the uncertainty of several parameters on the simulation results. We then simulated the debris flow at the Atsumari River on 20 July 2003. The conclusions of this study can be summarized as follows:

- The simulated erosion and deposition distances of the debris flow agreed well with observed data when the concept of D_c was included in the simulation. For simulations excluding this concept, there was little agreement with the observed erosion and deposition distances. Therefore, the hypothesis that fine sediments in large-scale debris flows behave like fluids was confirmed for the July 2003 debris flow at the Atsumari River.
- The D_c of 20 mm that we used in our numerical simulation was verified as a reasonable estimate of the particle size below which particles behaved like fluids for the 2003 debris flow at Atsumari River by comparison of the settling velocity of the D_c fraction with the friction velocity of the debris flow and the turbulent velocity of the interstitial water.

	Value	Method
Settling velocity	37 cm/s	Calculated from Eq. 17 (Rubey, 1933)
Friction velocity	164 cm/s	Calculated from river bed shear stress (Eq. 18)
Turbulent velocity	80 cm/s	Calculated from turbulent stress (Eq. 19)

Tab. 2 - Determination of settling, friction, and turbulent velocities

REFERENCES

- ASHIDA K., YAJIMA K. & TAKAHAMA J. (1989) – *Constitutive equation of debris flow*. Annuals of Disaster Prevention Research Institute, Kyoto University, **32** (B-2): 487-501, Japan.
- EGASHIRA S., HONDA N. & MIYAMOTO K. (1998) – *Numerical simulation of debris flow at the Gamaharazawa in the Hime river basin*. Annual Journal of Hydraulic Engineering, JSCE, **42**: 919-924, Japan.
- HOTTA N., MIYAMOTO K., SUZUKI M. & OHTA T. (1998) – *Pore-water pressure distribution of solid-water phase flow in a rolling mill*. Journal of the Japan Society of Erosion Control Engineering, **50**(6): 11-16, Japan.
- IVERSON R.M. & DENLINGER R.P. (2001) - *Flow of variably fluidized granular masses across three-dimensional terrain: 1. Coulomb mixture theory*. Journal of Geophysical Research, **106**(B1): 537-552.
- NAKAGAWA H., TAKAHASHI T., SATOFUKA Y., TACHIKAWA Y., ICHIKAWA Y., YOSHIDA Y. & NAKAMURA Y. (1998) – *Debris flow disasters at Harihara River*. Izumi City, Kagoshima Prefecture, 1997. Annuals of Disaster Prevention Research Institute, Kyoto University, **41** (B-2): 287-298, Japan.
- NAKAGAWA H., TAKAHASHI T., SATOFUKA Y. & KAWAIKE K. (2001) – *Sediment disaster caused by the heavy rainfall in the Camuri Grande River Basin, Venezuela, 1999-Repoduction of sediment runoff, flooding, and evaluation of effectiveness of the sabo works by means of numerical simulation*. Annuals of Disaster Prevention Research Institute, Kyoto University, **44** (B-2): 207-228, Japan.
- NAKATANI K. (2010) – *Development and Application of debris flow numerical simulation system equipped with a graphical user interface*. Ph.D Thesis, Kyoto University, Japan
- NAKATANI K., WADA, T., SATOFUKA Y., & MIZUYAMA T. (2008) – *Development of “Kanako 2D (Ver.2.00),” a user-friendly one- and two-dimensional debris flow simulator equipped with a graphical user interface*. International Journal of Erosion Control Engineering, **1**(2): 62-72, Japan.
- NAKATANI K., WADA, T., SATOFUKA Y., & MIZUYAMA T. (2009) - *Study on preventing debris flow disaster on heritage existing mountainous area applying numerical simulation*. Disaster Mitigation of Cultural Heritage and Historic Cities, **3**: 135-142, Japan.
- O'BRIEN J.S., JULIEN P.Y. & FULLERTON W.T. (1993) – *Two- dimensional water flood and mudflow simulation*. J. Hydraulic Engineering, **119** (2): 244-261.
- RICKENMANN D, LAIGLE D, McARDELL B.W. & HÜBL J. (2006) - *Comparison of 2D debris-flow simulation models with field events*. Computational Geosciences, **10**: 241-264.
- RUBEY W.W. (1933) – *Settling velocities of gravel, sand and silt particles*. American Journal of Science, **25**: 325-338.
- TAKAHAMA J., FUJITA Y., KONDO Y & HACHIYA K. (2002) - *Two-layer model for analysis of deposition and erosion processes of debris flows*. Annual Journal of Hydraulic Engineering, JSCE, **46**, 677-682, Japan.
- TAKAHASHI T. (1977) – *Mechanism of occurrence of mud–debris flows and their characteristics in motion*. Annual of Disaster Prevention Research Institute, Kyoto University, **20** (B-2): 405-435, Japan.
- TAKAHASHI T. (2004) – *Mechanics and countermeasure of debris flow*. Kinmirai-sha, Japan.
- TAKAHASHI T. & KUANG S. (1986) – *Formation of debris flow on varied slope bed*. Annuals of Disaster Prevention Research Institute, Kyoto University, **29** (B-2) : 345-359, Japan.
- TAKAHASHI T & NAKAGAWA H. (1991) – *Prediction of stony debris flow induced by severe rainfall*. Journal of the Japan Society of Erosion Control Engineering, **44**(3): 12-19, Japan.
- TAKAHASHI T., SATOFUKA Y & CHISHIRO K. (1996) – *Dynamical law of debris flows in inertial regime*. Annual of Disaster Prevention Research Institute, Kyoto University, **39** (B-2): 333-346, Japan